Stability behavior of anionic spherical polyelectrolyte brushes in the presence of La(III) counterions

Christian Schneider,[1] Arben Jusufi,[2] Robert Farina,[3] Philip Pincus,[3] Matthew Tirrell,[3,4,*] and Matthias Ballauff[5,6,†]
[1]*Physikalische Chemie I, University of Bayreuth, 95440 Bayreuth, Germany*
[2]*Institute for Computational Molecular Science, Temple University, Philadelphia, Pennsylvania 19122-6081, USA*
[3]*Departments of Chemical Engineering and Materials, Materials Research Laboratory, University of California–Santa Barbara, Santa Barbara, California 93106-2050, USA*
[4]*Department of Bioengineering, Chemical Engineering and Materials Science & Engineering, Materials Science Division, Lawrence Berkeley National Laboratory, University of California–Berkeley, Berkeley, California 94720-1762, USA*
[5]*F-I2 Soft Matter and Functional Materials, Helmholtz-Zentrum Berlin, Hahn-Meitner-Platz 1, 14109 Berlin, Germany*
[6]*Department of Physics, Humboldt University Berlin, Newtonstr. 15, 12489 Berlin, Germany*
(Received 5 March 2010; published 7 July 2010)

In this paper we discuss the stability behavior of spherical polyelectrolyte brushes (SPB) in the presence of trivalent lanthanum counterions. Stability behavior is measured through the rate of coagulation of the SPB as a function of the lanthanum concentration using simultaneous static and dynamic light scattering. As the counterion concentration increases, we observe coagulation of the SPB which in turn leads to a dramatic decrease in the stability of our particles. Since the rate of coagulation is dependent upon the balance between the repulsive interactions and the thermal energy of the diffusing particles (reaction-limited colloidal aggregation; RLCA), we then can relate the measured particle stability to the value of the repulsive potential in the RLCA regime. These "microsurface potential measurements" (MSPM) allow us to measure repulsive energies down to the order of k_BT. From the repulsive energy of the particles we can then determine precise information about the net surface potential Ψ_0 of the SPB as a function of the lanthanum counterion concentration. Moreover, we demonstrate that a simple mean-field model predicts the stability of the SPB in the presence of lanthanum counterions with high accuracy.

DOI: 10.1103/PhysRevE.82.011401 PACS number(s): 82.70.−y, 64.70.pv, 64.75.Gh, 64.75.Xc

I. INTRODUCTION

Colloidal dispersions consisting of solid nanoparticles dispersed in water present one of the most studied systems in colloid science [1]. In principle these systems are metastable, that is, the particles will aggregate if insufficient stabilization is present [2]. Stabilization can be achieved in two ways: Either charges are affixed to surfaces of the particles (electrostatic stabilization) or the particles can carry long polymer chains (steric stabilization) [3]. Individually, both modes of stabilization are now rather well understood. In particular, electrostatic stabilization can be cast into the well-known Derjaguin-Landau-Verwey-Overbeek (DLVO) theory [4,5] which allows a detailed prediction of colloidal stability in the presence of multivalent salt ions with valency z of a given critical concentration n_{crit}. Here the empirical Schulze-Hardy rule states that $n_{crit} \propto z^{-6}$ in direct agreement with the DLVO-theory [6].

Much less is known about electrostatic stabilization that results from appending charged polymer chains to the surface of colloidal spheres. Here, electrostatic and steric effects are combined to create the so called electrosteric stabilization. This electrosteric stabilization is the basis of many industrial polymer dispersions [7]. Hence, a profound understanding of electrosteric stabilization is of central technological importance. It is also important to note, that many applications in medicine and personal care products operate in multivalent ionic media. Spherical polyelectrolyte brushes (SPB) that consist of solid colloidal spheres onto which long chains of a polyelectrolyte are appended present excellent model systems for an in-depth study of electrosteric stabilization [8]. Figure 1(a) displays the structure of these particles in a schematic fashion. The term brush indicates a grafting density of the appended chains that is dense enough to ensure strong lateral interactions among the polyelectrolyte chains [9]. The main feature of polyelectrolyte brushes is the strong confinement of the counterions within the brush layer, first predicted by Pincus [10] as well as Birshtein, Borisov, and Zhulina [11]. If monovalent counterions are present, the high number of charges confined in such a polyelectrolyte brush will lead to a strong stretching of the attached chains in order to alleviate the concomitant osmotic pressure of the counterions. If the ionic strength is raised in this system by adding monovalent salt, the height of the polyelectrolyte layer will decrease considerably [12,13]. However, the colloidal stability remains unimpeded as experimental studies have demonstrated that the SPB are fully stable even in a three molar solution of monovalent salt [13]. The results regarding the salt dependency of the brush height obtained for the spherical systems are in qualitative agreement with direct measurements using the surface forces apparatus (SFA) [14,15].

An entirely different situation arises if di- or trivalent salt is added to aqueous solutions of spherical polyelectrolyte brushes. It has been demonstrated that rather moderate concentrations (0.1 mol/l) of divalent ions lead to the loss of

*mvtirrell@berkeley.edu
†matthias.ballauff@helmholtz-berlin.de

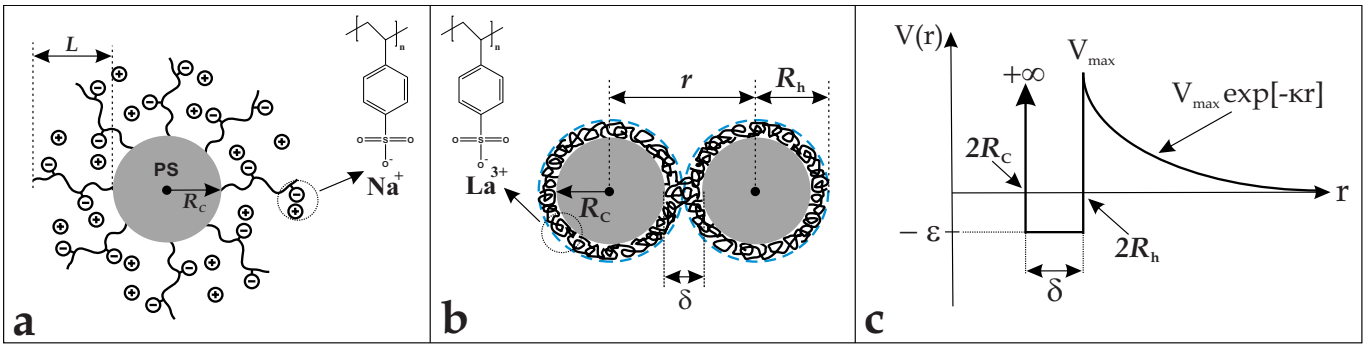

FIG. 1. (Color online) (a) Schematic representation of the spherical polyelectrolyte brush investigated in this study. Anionic polyelectrolyte chains are grafted from colloidal particles (radius: R_c=125 nm) made from solid poly(styrene). The particles are immersed in aqueous salt solutions with defined ionic strength. The thickness L of the brush layer is measured for different ionic strengths by dynamic light scattering. The ionic strength in the system is adjusted by changing the concentration of added salt. (b) Schematic of two aggregated SPB particles upon contact of their polyelectrolyte shells with fully collapsed brush layers. The particle-particle center distance r equals $2R_h=2R_c+\delta$ where δ is twice the brush thickness L. In all concentrations of lanthanum ions used here the hydrodynamic radius R_h of the particles is constant. (c) Interaction potential of the SPB particles in the aqueous lanthanum solutions used in our study [2].

colloidal stability and to the flocculation of particles [12]. In the case of trivalent ions, minute concentrations are sufficient to induce flocculation [16]. Concomitantly, the polyelectrolyte chains collapse to form a rather dense layer that does not provide any steric stabilization [2]. Hence, results obtained in the presence of monovalent counterions show a strong stability of the SPB, while minute concentrations of trivalent ions lead to rapid flocculation. As has been discussed recently [16], the height L of the brush layer affixed to the surface of the particles can be quantitatively understood in terms of a simple model [17], if ion specific interactions with the polyelectrolyte chains as observed, e.g., for a poly(methacrylic acid) brush by Konradi and Rühe [18] can be neglected. L then results from a balance between the stretching of the chains due to the osmotic pressure of the counterions and the entropic retracting force of the coiled polymer chains. The results of this model are in excellent agreement with recent molecular dynamics (MD) simulations and experimental results [19,20]. An important assumption of this model is a strong electrostatic interaction between multivalent ions with the polyelectrolyte chains. Multivalent ions also replace an equivalent amount of monovalent ions and thus take away significant contributions to the osmotic pressure. This explains not only the strong reduction of L but suggests also a qualitative explanation of the decreased colloidal stability of the SPB in the presence of multivalent ions [19]. In our study we use rather high concentrations of lanthanum counterions which leads to two primary effects: firstly, the shell layers of the SPB are always completely collapsed, and secondly, the shell layers of the SPB stick to each other upon contact [2].

In a recent paper, we demonstrated that the rate of coagulation can be used to assess the repulsive force in the particle interaction potential $V(r)$ between two colloidal particles [2]. The central idea is depicted in Fig. 1. The surfaces of two SPB can approach each other to a certain minimum distance $\delta=2L$. In this configuration, the potential $V(r)$ is at a maximum value $V_{max}=V(2R_c+\delta)$ with R_c as the particle core radius. Therefore, V_{max} presents the maximum barrier that needs to be overcome by thermal motion to achieve contact between two particles in the fully collapsed state. In the presence of moderate concentrations of multivalent salt, two particles will stick to each other essentially irreversibly once their surfaces have touched [21]. Therefore, the rate of coagulation leads to direct information on the potential $V(r)$ and in particular on V_{max}. The basic theory of the rate of coagulation is well known: if $V_{max}=0$, the limiting case of the diffusion-limited colloidal aggregation (DLCA) is reached [6]. For $V_{max}>0$, the rate of coagulation in this reaction-limited colloidal aggregation (RLCA) regime is much slower. For $V_{max}\gg k_BT$, coagulation is slow enough that the suspension appears stable.

Up until now, careful measurements of the kinetics of coagulation have been used to test given interparticle potentials, for example the well-known DLVO-potential [3,22]. Borkovec and coworkers then demonstrated that the rate of coagulation can be obtained very accurately by a combination of static and dynamic light scattering [23,24]. However, the procedure can be reversed. First, we measure the formation rate of particle doublets. Applying the interparticle potential of fully collapsed polyelectrolyte brushes then leads to $V(r)$ and in particular V_{max} of the SPB. These 'micro surface potential measurements' (MSPM) hence supplement the classical methods used for obtaining the repulsive pair potential. This has been done through experimental methods such as the SFA [14,25,26], optical tweezers [27–29], the total internal reflection microscopy (TIRM) [30–32], and the colloidal probe atom force microscopy (AFM) [33–35]. In particular, MSPM allow us to assess the repulsive potential $V(r)$ between colloidal particles of arbitrary size down to the theoretical limit, $V_{max}\approx k_BT$. In general, MSPM give precise information about the maximum of the repulsive interaction V_{max}. In many cases, the functional dependence of the potential on r is known or can be found through measurements with parallel surfaces using the SFA. With this information, MSPM can lead to a full comparison between theory and experiment [2].

With this work we wish to extend our previous work on MSPM and to expand the discussion of the method used. Moreover, a critical comparison of the theoretical model for

$V(r)$, which has been developed recently for SPB, will be given [2]. While our previous work was confined to the domain of weak repulsion, a stability ratio W close to unity, we shall discuss data of much more stable systems in which $W \approx 10^3$. Our comparison between theory and experimental work will thus provide a means to investigate electrosteric stabilization more thoroughly.

The paper is organized as follows: after the Experimental Section the theory related to the kinetics of coagulation will be reviewed. We then further investigate our theoretical model used for a comparison with experimental data. The subsequent section Results and Discussion, will first present the kinetic analysis of coagulation. This will be followed by an in-depth discussion of the comparison of this data with our theoretical model. A short conclusion will sum up the main points of this work.

II. EXPERIMENTAL SECTION

A. Materials and Methods

Materials. All solvents were analytical grade and used as received. Styrene (Sigma-Aldrich) was distilled under reduced pressure to remove inhibitor molecules and stored under nitrogen at 4 °C until used. Sodium styrene sulfonic acid (Fluka), potassium persulfate (Merck), sodium bicarbonate (Grüssig), sodium bisulfite (Merck) and lanthanum(III)chloride heptahydrate (Sigma-Aldrich) were used without further purification. The synthesis of the photoinitiator 2-[p-(2-hydroxy-2-methylpropiophenone)]-ethyleneglycol-methacrylate (HMEM) was performed according to the method used by Guo *et al.* and purified chromatographically [36]. In all experiments we used water obtained from a Millipore ion exchange apparatus.

Instrumentation. For the dynamic light scattering (DLS) measurements and the simultaneous static and dynamic light scattering experiments we used an ALV-4000 goniometer with a 35 mW He-Ne laser operating at a wavelength of 632.8 nm, an ALV/High QE APD detector and an ALV-6010/160 External Multiple Tau Digital Korrelator unit. This setup was then able to obtain measurements at 10 s intervals using absolute particle concentrations as low as 10^{13} per m^3 at scattering angles between 20° and 150°.

Determination of the molecular weight and molecular weight distribution of the poly(styrene sulfonate) (PSS) chains was performed using aqueous gel permeation chromatography (GPC). We used linear poly(sodium styrene sulfonate) to construct a universal master curve. As eluent we used water at pH 9. For evaluation of the eluent we used an Agilent 1100 differential refractometer RID detector.

Transmission electron microscopy (TEM) images were prepared on a Zeiss CEM 902 instrument operating at an accelerating voltage of 80 kV. One drop of the aqueous suspensions (0.1% solid content) was deposited onto a copper grid coated with carbon (Plano) and air-dried at room temperature. The images were recorded digitally by a MegaView3 camera. We used the program IMAGEJ 1.37v (RSB, National Institute of Mental Health) for manually counting the mapped particles.

Synthesis of the SPB. The synthesis of the SPB follows the route mapped out by Wittemann *et al.* for anionic systems [37], with the exception of using sodium styrene sulfonic acid as the comonomer and emulsifier in the emulsion polymerization of the core particles. Thus, the synthesis of the core is an emulsifier-free emulsion polymerization. The solid content in the emulsifier-free emulsion polymerization was chosen to be 12.5%. The amounts of sodium styrene sulfonic acid and other additives were chosen to yield core diameters of about 200 nm [38]. Before and after the photo emulsion polymerization of the PSS shell, the suspension was cleaned by a serum replacement with water. It should be noted that we avoided the use of detergent solution for the cleaning of instruments and equipment during the entire synthesis process of the SPB. Instead we used pure organic solvents and a mixture of isopropanol and potassium hydroxide. In this way, contamination of the system by surfactants was circumvented.

Characterization of the SPB. The hydrodynamic radius of the core R_c was (125 ± 2) nm, which was measured by DLS in water at very low ionic strength via cumulant analysis using the third cumulant and the Einstein-Stokes relationship [39]. The hydrodynamic radius of the SPB particles at very low ionic strength was (190 ± 2) nm, which includes the hydrodynamic shell thickness L of (65 ± 3) nm and the hydrodynamic radius of the core R_c. Note however, that this value strongly decreases in the presence of the multivalent lanthanum counterions. For the DLS measurements the suspensions were filtered through a 1 μm PES filter. TEM gave a radius of 113.8 nm and a polydispersity index of 1.0001 for the core particles, for which we evaluated over 750 particles. The difference between the core radii values may be attributed to short polymer chains of comonomer on the surface of the core particles, the presence of the electric double layer or very weak coagulation during the cleaning process. However, the difference does not play an essential role regarding the results shown here.

After cleaving off the chains from the core particles we determined the molecular weight distribution by GPC [37]. The contour length L_c of the chains was estimated using the molecular weight of $(67{,}500 \pm 13{,}500)$ g/mol of the longest chains in the shell layer. This yielded (82 ± 16) nm for L_c, where the monomer size has been estimated to be 0.25 nm. The mass ratio between the core and the shell m_c/m_s of the SPB was (12 ± 3) as determined by gravimetry. Considering m_c/m_s and the molecular weight of the longest polyelectrolyte chains of $(67\,500 \pm 3500)$ g/mol we calculated a grafting density σ of (0.03 ± 0.01) chains per nm^2. Using the mass ratio m_c/m_s we also calculated the number of charged units per SPB particle to $Q(\mathrm{NaSS}) = (1\,840\,000 \pm 644\,000)$.

The absolute number concentration $[P]_0$ of the SPB suspension after the photo emulsion polymerization was $(3.47 \pm 0.58) \times 10^{18}/m^3$. We calculated the particle concentration using the solid content of the suspension determined by gravimetry and the size of the core particles determined via TEM. We also accounted for the weight of the shell layer of the SPB using the mass ratio m_c/m_s. For calculating the weight of the core particles we assumed a uniform density of 1.054 g/cm^3, which is the polystyrene bulk density [40].

Methods. The investigation of the coagulation kinetics of

the SPB was performed using simultaneous static and dynamic light scattering as described by Holthoff and coworkers [23]. Our experiments also contained $LaCl_3$ in the concentration range of 0.16 to 150 mmol/l. In order to obtain a good signal for every salt concentration, we varied the absolute particle concentration between $(1.35 \pm 0.23) \times 10^{13}/\mathrm{m}^3$ at high electrolyte concentrations and $(8.00 \pm 1.36) \times 10^{15}/\mathrm{m}^3$ at low electrolyte concentrations. This particle concentration range was low enough to avoid multiple scattering [23]. All measurements of the stability ratio were performed at a scattering angle of 90°. For the determination of the Rayleigh-Debye (RD) form factor of the SPB, we used an absolute particle concentration of $(3.00 \pm 0.51) \times 10^{14}/\mathrm{m}^3$ and electrolyte concentrations of 1 mmol/l and 5 mmol/l at scattering angles between 20° and 150°. In all cases, the temperature during the light scattering measurements was 25 °C.

The light scattering cells were cleansed regularly with chromium sulfuric acid to eliminate organic residues. Between measurements, the light scattering cells were flushed several times with water and electrolyte solution before reuse. We compared the initial radius of the SPB particles of each individual measurement and found no major deviations. We also had high reproducibility of the fits of both the hydrodynamic and static light scattering experiments.

We prepared two different stock solutions with the absolute number concentrations of $(2.25 \pm 0.28) \times 10^{16}/\mathrm{m}^3$ and $(3.47 \pm 0.59) \times 10^{17}/\mathrm{m}^3$, respectively. Coagulation was then initiated by adding a latex stock solution (in the range of 15–40 μl) to an electrolyte solution (in the range of 1.3–2.6 ml) in the light scattering cell. The same latex stock solutions were used for all coagulation measurements. Data were collected at 10 s intervals to yield a data point for both the hydrodynamic radius and the scattering intensity at time t. In the dynamic light scattering measurements, we fit the autocorrelation function with a nonlinear square fit using a third-order cumulant expansion with an adjustable baseline to yield one data point. The values for the hydrodynamic radius were calculated out of the first cumulant and through the use of the Stokes-Einstein relationship. For this calculation we have taken into account changes in the viscosity based on electrolyte concentration [41]. In the static light scattering measurements, we calculated the time average of the scattering intensity to give one data point every 10 s. For one coagulation measurement, we combine approximately 150–1000 static and dynamic data points.

For all electrolyte concentrations and scattering angles, we determined the coagulation rate constant k_{11} using Eq. (1). In order to obtain the initial slope, we fit a second degree polynomial to the static and dynamic data. Extrapolating the fits to time zero yields the values of the hydrodynamic radius $R_h(0)$ and the scattering intensity $I(0)$. Due to the fact, that the lanthanum concentrations were high, the shell layer of the SPB particles was always completely collapsed. Therefore, we could determine the mean hydrodynamic radius of the collapsed SPB, $R_{h,csl}$, by averaging the values of $R_h(0)$ of all lanthanum concentrations. This yields (137 ± 3) nm for $R_{h,csl}$. The error is the standard deviation of the individual values. Subtracting the hydrodynamic core radius of the particles gives the mean hydrodynamic shell thickness of the SPB, L. The radius of the single particles $R_{h,1}$ is assumed to be given by the hydrodynamic radius at time zero, so that $R_{h,1}=R_h(0)$.

The method of Holthoff and co-workers [23] is strictly valid only at the initial stage of the coagulation process where only doublets are formed. Therefore, we considered only data points up to the point where $R_h(t)=1.2\ R_h(0)$ for evaluation. We calculated the stability ratio using the equation $W=k_{11}[c(\text{electrolyte})=150\ \text{mmol/l}]/k_{11}[c(\text{electrolyte})]$ where every measurement of $k_{11}[c(\text{electrolyte})]$ was repeated at least three times. Averaging all coagulation rate constants in the fast regime yielded the experimental fast coagulation rate constant.

We determined the relative form factors as a function of the scattering angle using Eq. (2) for the dynamic data to yield $I_2/2I_1$ and Eq. (3) for the static measurements to give $(I_2/2I_1)-1$, where I_1 and I_2 are the singlet and doublet light scattering intensities, respectively. In both cases, we calculated k_{11} out of each individual measurement from Eq. (1). Again, we repeated the measurements at every scattering angle at least 3 times.

B. Simultaneous static and dynamic light scattering

The coagulation rate constant k_{11} of colloidal particles can be precisely determined by simultaneous static and dynamic light scattering [23]. Measurements of the change of the hydrodynamic radius dR_h and the scattering intensity dI during the coagulation process as a function of the time at an arbitrary scattering angle can be evaluated through [23]

$$k_{11}[P]_0 = \frac{R_{h,2}}{R_{h,2}-R_{h,1}}\left(\frac{dR_h(t)/dt}{R_h(0)}\right) - \left(\frac{dI(q,t)/dt}{I(q,0)}\right), \quad (1)$$

where $[P]_0$ is the initial particle concentration, $R_{h,1}$ and $R_{h,2}$ are the hydrodynamic radii of single spheres and doublets, respectively, $R_h(t)$ is the hydrodynamic radius of the particles at a specific time t and $I(t,q)$ is the angle dependent scattering intensity of the suspension at time t. The doublet hydrodynamic radius is calculated using the equation $R_{h,2}=1.38\ R_{h,1}$ as introduced by the work of Borkovec and coworkers [23]. Within the Rayleigh-Debye approximation, the initial change of the hydrodynamic radius at an arbitrary scattering vector q is given by [42]

$$\frac{1}{R_h(0)}\left(\frac{dR_h(t)}{dt}\right)_{t\to 0} = \frac{I_2(q)}{2I_1(q)}\left(1-\frac{R_{h,1}}{R_{h,2}}\right)k_{11}[P]_0 \quad (2a)$$

$$= \left(\frac{\sin(2aq)}{2aq}+1\right)\left(1-\frac{R_{h,1}}{R_{h,2}}\right)k_{11}[P]_0, \quad (2b)$$

where a is the radius of the primary particles and $q=4\pi n/\lambda \sin(\theta/2)$. Here, n is the refractive index of the medium, λ is the wavelength of the incident beam and θ is the scattering angle. The static light scattering data allows the determination of the optical factor $[I_2(q)/2I_1(q)]-1$ using [42]

$$\frac{1}{I(q,0)}\left(\frac{dI(q,t)}{dt}\right)_{t\to 0} = \left(\frac{I_2(q)}{2I_1(q)} - 1\right)k_{11}[P]_0 \tag{3a}$$

$$= \left(\frac{\sin(2aq)}{2aq}\right)k_{11}[P]_0. \tag{3b}$$

III. THEORY

A. Coagulation kinetics of SPBs

The coagulation rate constant k_{11} for the formation of doublets from singlet particles undergoing Brownian motion is defined through [43]

$$\frac{d[P]}{dt} = k_{11}[P]^2, \tag{4}$$

where $[P]$ is the singlet particle concentration at a given time t [6]. In the present work the doublet formation is assumed to be irreversible. If no repulsive forces hinder the coagulation of the particles, the coagulation process is controlled entirely by Brownian motion. For this diffusion limited, or fast coagulation process, the theory of von Smoluchowski predicts a coagulation rate constant $k_{11,Sm}$ of [44,45]

$$k_{11,Sm} = \frac{4k_BT}{3\eta}, \tag{5}$$

where k_BT is the thermal energy of the particles and η is the viscosity of the fluid. In the case of repulsive interaction between the particles, only the fraction $1/W$ of all singlet collisions results in the formation of doublets. W is the stability ratio, which is defined as the ratio of the rate constant of rapid coagulation $k_{11,fast}$ and the rate constant for particles with nonzero repulsion $k_{11,slow}$ [6]

$$W = \frac{k_{11,fast}}{k_{11,slow}}. \tag{6}$$

Note that for the experimental determination of W we assume $k_{11}(c_0 = 150\ \text{mmol/l}) = k_{11,fast}$. In the slow coagulation regime, the stability ratio is a function of the total interaction potential $V(r)$ and must include a correction function $B(r)$, which accounts for the hydrodynamic interactions between the two colliding particles in the process of aggregation. Using $B(r)$, W is then described by [46]

$$W \equiv \frac{\int_{2R}^{\infty} B(r)\exp\left(\frac{V(r)}{k_BT}\right)r^{-2}dr}{\int_{2R}^{\infty} B(r)\exp\left(\frac{V_A(r)}{k_BT}\right)r^{-2}dr}, \tag{7}$$

where R is the radius of the spheres, $V_A(r)$ is the interaction potential including only attractive forces and r is the particle-particle center distance. Here, the correction function for the hydrodynamic drag $B(r)$ is given as [24]

$$B(r) = \frac{6\left(\frac{r-2R}{R}\right)^2 + 13\left(\frac{r-2R}{R}\right) + 2}{6\left(\frac{r-2R}{R}\right)^2 + 4\left(\frac{r-2R}{R}\right)}. \tag{8}$$

The double layer interaction between two charged spheres can be calculated in terms of the weak-overlap-approximation [47]. For two charged spheres in the presence of a 3:1 electrolyte solution, the interaction potential results to

$$V_{2s}(r-2R_h) = \frac{24\pi R_h c_0 (e\Psi_0)^2}{\kappa^2 k_B T}\exp[-\kappa(r-2R_h)] \equiv V_{max}\exp[-\kappa(r-2R_h)], \tag{9}$$

where Ψ_0 is the effective surface potential, c_0 is the electrolyte number concentration in the solution, e is the charge of an electron and R_h is the hydrodynamic radius of the particles. Note that Eq. (9) is only valid if $\kappa R_h \gg 1$ and $e\Psi_0/k_BT < 1$. In this work both conditions are fulfilled [48]. The double layer interaction potential decreases exponentially with growing particle separation from its maximal value V_{max} defined through Eq. (9). The Debye screening length $1/\kappa$ is related to c_0 according to [6]

$$1/\kappa^2 = \epsilon\epsilon_0 k_BT/\sum_i (z_i e)^2 c_{0,i}, \tag{10}$$

where ϵ_0 is the permittivity of vacuum, ϵ is the relative dielectric permittivity of water, z_i is the valency and $c_{i,0}$ the number concentration of the ion species i.

We also must modify Eq. (9) in regard to the attractive van der Waals forces. Taking into account retardation effects, the van der Waals interaction of the solid poly(styrene) core of the SPB is given by [49]

$$V_{\text{vdW}}^{\text{core}}(r-2R_c) = -\frac{H_c R_c}{12(r-2R_c)}\left(1 - \frac{5.32(r-2R_c)}{\lambda_{\text{vdW}}}\times\ln\left[1 + \frac{\lambda_{\text{vdW}}}{5.32(r-2R_c)}\right]\right), \tag{11}$$

where H_c denotes the Hamaker constant of the particle cores, R_c is the radius of the poly(styrene) core of the particles and λ_{vdW} is the wave length of the van der Waals interactions. Following the literature, we set λ_{vdW} to 100 nm and H_c to 0.9×10^{-20} J [2,49]. The van der Waals interaction of two hollow shells $V_{\text{vdW}}^{\text{shell}}$ with shell thickness $\delta/2$ is given by [50]

$$V_{\text{vdW}}^{\text{shell}}(r-2R_h) = -\frac{H_s R_h}{12}\left(\frac{1}{(r-2R_h+\delta)} - \frac{2}{(r-2R_h+\delta/2)} + \frac{1}{r-2R_h}\right) - \frac{H_s}{6}\ln\frac{(r-2R_h)(r-2R_h+\delta)}{(r-2R_h+\delta/2)(r-2R_h+\delta/2)}, \tag{12}$$

where H_s is the effective Hamaker constant of the polyelectrolyte shells.

In the frame of the DLVO theory, superposition of Eqs. (9) and (11) leads to the interaction potential of charged hard spheres. The interaction potential of planar anionic polyelectrolyte brushes in the presence of $LaCl_3$ has previously been obtained by direct SFA measurements [2,21]. These SFA

measurements show an interaction potential which decreases exponentially with distance, as expected for electrostatic interaction [47]. However, upon contact of the two polyelectrolyte brushes a strong attractive force $-\varepsilon$ results. This strong attraction is due to intershell bridging of polyelectrolyte chains via the trivalent lanthanum counterions. The shape of force-distance curves measured by the SFA can be compared very closely with Fig. 1(c) as we see an exponentially increasing repulsive force followed by an adhesive force as the surfaces are separated. Thus, we obtain the interaction pair potential $V(r)$ of spherical polyelectrolyte brushes in the presence of $LaCl_3$

$$V(r) = \begin{cases} -\varepsilon & 2R_c \le r \le 2R_c + \delta \\ V_{max} e^{-\kappa(r-2R_c-\delta)} + V_{\mathrm{vdW}}^{\mathrm{core}}(r-2R_c) + V_{\mathrm{vdW}}^{\mathrm{shell}}(r-2R_c-\delta) & 2R_c + \delta \le r \end{cases}. \tag{13}$$

Here, r denotes the particle-particle center distance, δ is twice the thickness L of the collapsed shells and V_{max} is the prefactor of Eq. (9). In the case of SFA experiments, we can determine all of the parameters in Eq. (13) independently [2]. Note that in the case of only monovalent counterions, as pointed out in earlier studies with the SFA, forces between polyelectrolyte brush layers are always repulsive [14].

Even in the totally collapsed state (at high lanthanum concentrations) the polyelectrolyte shell layer consists mostly of water. Thus, the effective van der Waals force is close to zero. However, a certain degree of surface roughness of the collapsed shell layers and interparticle chain bridging must be taken into account. We therefore assume that a weak force is acting at very short particle separations due to the van der Waals force of the shell layers. We assume that $H_s = 10^{-4} H_c$, which is consistent with the SFA measurements [2]. The van der Waals force of the shell layers described by Eq. (12) is not corrected in regard to the retardation effect, due to the fact that the effective Hamaker constant of the shell layer is very small. At this point it is interesting to note, that the van der Waals force of the shell layers causes Eq. (16) to converge for $h \to 0$. Otherwise, the integral in Eq. (16) would diverge for $h \to 0$ because of $B(h)$. Thus, for core-shell systems the van der Waals attraction of the shell layers overcomes the repulsive hydrodynamic drag, which is expressed through $B(h)$, at separations <1 nm.

From Eq. (13) the definition of $V_A(r)$ follows naturally to

$$V_A(r) = \begin{cases} -\varepsilon & 2R_c \le r \le 2R_c + \delta \\ V_{\mathrm{vdW}}^{\mathrm{core}}(r-2R_c) + V_{\mathrm{vdW}}^{\mathrm{shell}}(r-2R_c-\delta) & 2R_c + \delta \le r \end{cases}. \tag{14}$$

We now calculate the stability ratio W as a function of the $LaCl_3$ concentration c_0 via Eq. (7) by using the interaction pair potential $V(r)$ of Eq. (13) and the attractive potential $V_A(r)$ according to Eq. (14). This leads to

$$W = \left\{ \int_{2R_c}^{2R_c+\delta} B(r) \exp\left[\frac{-\varepsilon}{k_B T}\right] r^{-2} dr + \int_{2R_c+\delta}^{\infty} B(r) \exp[\tilde{V}_{max} e^{-\kappa(r-2R_c-\delta)} + V_{\mathrm{vdW}}^{\mathrm{core}}(r-2Rc) + V_{\mathrm{vdW}}^{\mathrm{shell}}(r-2R_c-\delta)] r^{-2} dr \right\} \times \left\{ \int_{2R_c}^{2R_c+\delta} B(r) \exp\left[\frac{-\varepsilon}{k_B T}\right] r^{-2} dr + \int_{2R_c+\delta}^{\infty} B(r) \exp[V_{\mathrm{vdW}}^{\mathrm{core}}(r-2Rc) + V_{\mathrm{vdW}}^{\mathrm{shell}}(r-2R_c-\delta)] r^{-2} dr \right\}^{-1} \tag{15}$$

with $\tilde{V}_{max} = V_{max}/k_B T$. The first integrals in both the numerator and the denominator do not significantly contribute to the stability ratio, because $\delta \ll 2R_c$ and ϵ is not very negative at the initial contact of the particle surfaces. This can be reasoned from the SFA measurements [2]. Therefore, only the second integrals in Eq. (15) need to be taken into account. In Eq. (15), one has to substitute the particle-particle center distance by $r = h + 2R_c + \delta$ where h is the separation distance between the brush surfaces and $\delta = 2(R_h - R_c)$ [Fig. 1(b)]. Now Eq. (15) reads

$$W = \frac{\int_0^{\infty} B(h)(h+2R_h)^{-2} \exp[\tilde{V}_{max} e^{-\kappa h} + V_{\mathrm{vdW}}^{\mathrm{core}}(h+\delta) + V_{\mathrm{vdW}}^{\mathrm{shell}}(h)] dh}{\int_0^{\infty} B(h)(h+2R_h)^{-2} \exp[V_{\mathrm{vdW}}^{\mathrm{core}}(h+\delta) + V_{\mathrm{vdW}}^{\mathrm{shell}}(h)] dh}. \tag{16}$$

In this way, the stability ratio W of the SPB can be calculated at arbitrary Debye lengths $1/\kappa$ by numerical integration of Eq. (16).

B. Mean field model

In order to predict the stability ratio W through Eq. (16) the van der Waals interactions and the prefactor $\tilde{V}_{max}=V_{max}/(k_BT)$ of the electrostatic barrier potential is required. Due to the fact that the contribution of the van der Waals interactions are given by Eqs. (11) and (12), we only have to calculate V_{max} to predict W of the SPBs. According to its definition in Eq. (9), the relevant quantity is the surface potential Ψ_0, and ultimately, the effective surface charge density $\Sigma=Q^*/[4\pi(R_c+L)^2]$ of the SPB as outlined earlier [2]. There we used an approximate solution for the relation of Ψ_0 with the surface charge density Σ [51]. However, this approximation is valid only for $\kappa(R_c+L)>2$. For the smaller values of $\kappa(R_c+L)$, the analytical approximation of the Poisson-Boltzmann solution given by Zhou can be used [52]. It is accurate to less than 5% for $\kappa(R_c+L)>0.03$. In the following, the details of the model calculation will be given. We start with the determination of the surface charge density Σ. For this, the net charge Q^* and the brush thickness L were calculated for each salt concentration. Both quantities can be determined through a variational free energy approach that was originally applied on polyelectrolyte stars [53,54]. This cell model can be extended to SPB by taking into account a core of finite size [17]. In previous studies we showed, that the mean-field model successfully describes the results of computer simulations [19], the collapse of the brush height [16], and the effective charge of SPBs [2,20] in the presence of multivalent counterions for SPBs of various dimensions.

The free energy of an isolated SPB with a core radius R_c, number of chains f, a degree of polymerization D_p and a brush thickness L, in correspondence to a given density, consists of the following contributions:

A Hartree-type contribution describes the electrostatic potential of the SPB with a net charge Q^* [17],

$$\frac{U_H}{k_BT}=\frac{Q^{*2}\lambda_B}{2e^2}u(L;R_w,R_c) \tag{17}$$

with λ_B being the Bjerrum length (0.72 nm for water at 298 K). The function $u(L;R_w,R_c)$ contains the dependency on the brush thickness L, and on the size parameters R_c and the Wigner-Seitz cell radius R_w, see Ref. [17] for more details. This function $u(L;R_w,R_c)$ depends on the charge distribution in- and outside of the brush. For monovalent counterions a parabolic decay of the charge density has been proven to be an accurate description [54,56–59]. For the present case that contains mainly multivalent counterions the exact form of the charge distribution inside the brush is of minor importance, since the shell layer thickness is very small compared to the overall dimension of the SPB $(L/(R_c+L)\ll 0.1)$ [60].

The next free energy contribution accounts for the entropic terms of the counterions and coions [55]. It is a reasonable approximation to consider all absorbed multivalent counterions as being osmotically inactive due to their strong correlation to the chains [19,56]. Outside the brush there is a mixture of the monovalent counterions coming from the brush ($N_+=|Q_b|/e$; Q_b is the bare charge of the SPB), multivalent counterions $[N_z=c_0V_w-|Q_b-Q^*|/(ez)]$ and coions $(N_{co}=zc_0V_w)$, where c_0 is the number density of $LaCl_3$ salt, $V_w=(4\pi/3)R_w^3=1/\rho_{SPB}$ which corresponds to the free volume of each SPB at a given SPB density ρ_{SPB} and l_0 is the monomer size (0.25 nm). Here Q_b is given by the number of charged units per SPB Q(NaSS). Note that all monovalent counterions are completely replaced by trivalent ones and the net charge is determined through the remaining trivalent ions outside the SPB. Inside the brush there are $|Q_b-Q^*|/(ez)$ multivalent ions. The coions do not enter the brush regime in our model. It has been shown that this is a reasonable approximation due to electrostatic repulsions between coions and the SPB [54]. Consequently there is only one entropic contribution from the free ions

$$\frac{S}{k_BT}=(N_{co}+N_++N_z)\left[\ln\left(\frac{N_{co}+N_++N_z}{V_w}l_0^3\right)-1\right]. \tag{18}$$

The remaining free energy contributions result from the chains [61,62]. A contribution related to the elastic energy of the brush chains can be written as

$$\frac{F_{el}}{k_BT}=\frac{3fL^2}{2D_pl_0^2}, \tag{19}$$

which stems from a Gaussian approximation of the conformational entropy of the brush chains, while the self-avoidance is accounted by a Flory-type expression

$$\frac{F_{Fl}}{k_BT}=\frac{3v(fD_p)^2}{8\pi[(R_c+L)^3-R_c^3]} \tag{20}$$

with the excluded volume parameter $v\approx l_0^3$. As usual for the case of good-solvent conditions, triplet-monomer contributions have been omitted.

The total free energy is obtained by adding up all contributions from Eqs. (17)–(20). This total free energy is minimized with respect to the net charge Q^* and the brush thickness L. Having calculated the brush thickness L and the net charge Q^* of the SPB, the surface potential can be readily obtained. For this we treat the SPB as a sphere with radius R_c+L and a surface charge density of $\Sigma=Q^*/[4\pi(R_c+L)^2]$ from which we determine the surface potential Ψ_0 using the asymptotic expression by Zhou [52]. In this way, one can predict the prefactor V_{max} and the stability ratio W at different salt concentrations using Eqs. (9) and (16), respectively, from the experimental parameters of the SPB, namely R_c, L_c, and σ.

IV. RESULTS AND DISCUSSION

A. Relative form factors

The main goal of this work was to measure exact coagulation rate constants of SPB particles using light scattering. We began by first investigating the dependence of $I(t)/dt$ and $R_h(t)/dt$ on the scattering vector q using simultaneous static and dynamic light scattering experiments in 1 and 5 mmol/l $LaCl_3$ solutions at scattering angles between 20° and 150°. Figure 2 displays the hydrodynamic radius $R_h(t)$ and the static light scattering intensity $I(t)$ as a function of the time t at a scattering angle of 90°. The change of $R_h(t)$ and $I(t)$ with t gives the absolute coagulation rate constant k_{11} for each

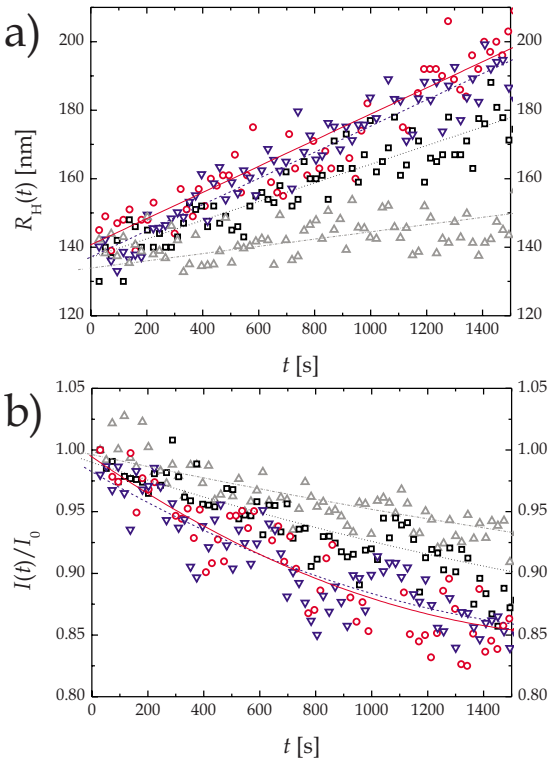

FIG. 2. (Color online) (a) The hydrodynamic radius $R_h(t)$ and (b) the normalized scattering intensity $I(q,t)/I_0(q)$ as a function of time for different lanthanum concentrations c_0 with linear and second order fits, respectively: 150 mmol/l (circles, solid line); 1 mmol/l (reversed triangles, broken line); 0.45 mmol/l (squares, dotted line); 0.21 mmol/l (triangles, broken dotted line). Here, the number concentration $[P]_0$ is 3.00×10^{14} m^{-3} and the scattering angle θ is 90°.

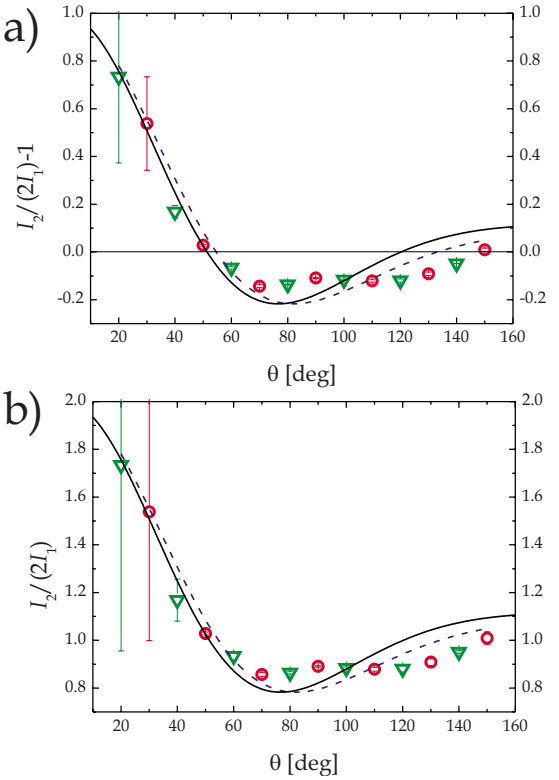

FIG. 3. (Color online) Relative doublet form factor $I_2(q)/[2I_1(q)]$ measured by (a) static and (b) dynamic light scattering. The solid line is calculated via the Rayleigh-Debye approximation using a particle singlet radius of 137 nm. The broken line shows the best fit with a singlet radius of 129 nm. The data points were obtained from multiangle simultaneous static and dynamic light scattering measurements in 1 mmol/l (reversed triangles) and 5 mmol/l (circles) $LaCl_3$ solutions. In all cases the number concentration is $[P]_0$: 3.00×10^{14} m^{-3}.

concentration of $LaCl_3$ by applying Eq. (1) to the data shown in Figs. 2(a) and 2(b). We first normalized $I(t)$ with the singlet form factor $I(t=0)$ and $R_h(t)$ with the initial hydrodynamic radius $R_h(t=0)$. The dependence on q of $I(t)/I(t=0)$ and $R_h(t)/R_h(t=0)$ are given by the optical factors $[I_2(q)/2I_1(q)]-1$ and $[I_2(q)/2I_1(q)]$ in Eqs. (3a) and (2a), respectively [23].

We calculated these optical factors as a function of the scattering angle using Eqs. (3) and (2) with $R_{h,csl}=137$ nm for the particle radius a in the Rayleigh-Debye (RD) approximation. The result is shown in Fig. 3. The theoretical curves deviate slightly from the experimental data points for both the static and dynamic light scattering measurements. These deviations are more pronounced at high values of q. The best theoretical fit of the data in Fig. 3 was obtained with $a=(129\pm3)$ nm, however discrepancies at high scattering angles still remain. The RD approximation is only valid in the limits of $|m-1|\leq1$ and $(4\pi a/\lambda)|m-1|\leq1$, where m is the ratio of the refractive index between the medium and the liquid [63]. In our case $|m-1|=0.2$ and $(4\pi a/\lambda)|m-1|=0.54$, so that both constraints are satisfied. However, since similar discrepancies were found for hard spheres as well [23,64], we conclude, that the RD-theory simply does not provide a better description of real data.

Due to the fact that the doublet form factor of the SPB is not well enough described by the RD theory, it is necessary to measure the coagulation rates without relying on the RD doublet form factor. Therefore, we only used simultaneous static and dynamic light scattering, which is independent of any particle form factors, for determining coagulation rate constants of the SPB. We also used $R_{h,csl}=137$ nm for the radius of the collapsed SPB particles in the following sections since it is directly derived from dynamic light scattering.

B. Stability ratio *W*

For determining the stability ratio of the SPB as a function of the $LaCl_3$ concentration, the coagulation rate constants were measured using static and dynamic light scattering at a scattering angle of 90°. The measurement data is shown in Fig. 2. It can be seen that the slopes of the hydrodynamic radius versus time curves increase with rising concentrations of lanthanum up to a concentration of 0.5 mmol/l. A further increase of salt concentration to 150 mmol/l does not result in a higher slope. This is a clear indication that these data are in the fast coagulation regime.

The resulting stability ratio is shown in Fig. 4. At $c_0(LaCl_3)=0.5$ mmol/l one observes a sharp transition from

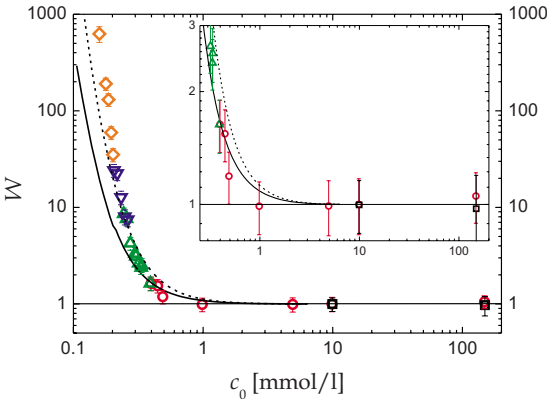

FIG. 4. (Color online) Stability ratio $W=k_{11}(c_0=150\ \text{mmol/l})/k_{11}(c_0)$ of the SPB as a function of the lanthanum concentration c_0 for different SPB concentrations $[P]_0$: 8.00×10^{15} m^{-3} (diamonds); 2.00×10^{15} m^{-3} (reversed triangles); 6.01×10^{14} m^{-3} (triangles); 3.00×10^{14} m^{-3} (circles); 1.40×10^{13} m^{-3} (squares). The scattering angle θ is 90°. The lines are the predictions from the mean-field theory for a SPB concentration of 6.01×10^{14} m^{-3}. The solid line shows the a priori predictions of W. The broken line is calculated by increasing the prediction of the effective charge of the SPB particles by 15%, as explained in Sec. IV B. The inset shows W for intermediate and high lanthanum concentrations only.

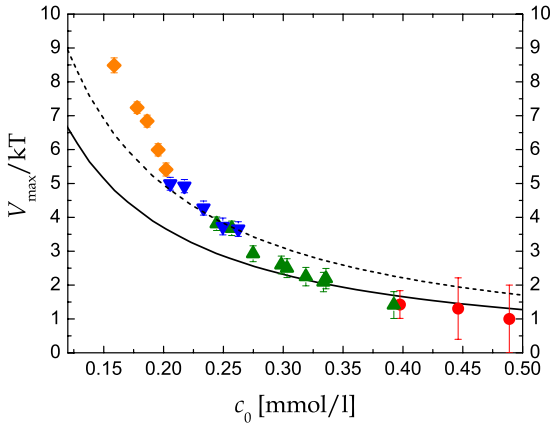

FIG. 5. (Color online) Prefactor $\tilde{V}_{max}=V_{max}/k_BT$ as a function of salt concentration c_0 of $LaCl_3$. Experimental data are shown for four different SPB concentrations $[P]_0$: 8.00×10^{15} m^{-3} (diamonds); 2.00×10^{15} m^{-3} (reversed triangles); 6.01×10^{14} m^{-3} (triangles); 3.00×10^{14} m^{-3} (circles). The data points were calculated from the experimental determined values of the prefactor $\tilde{V}_{max}$ using a particle radius $R_{h,csl}=137$ nm, corresponding to a thickness of the collapsed brush layer of 12 nm. The lines are the predictions from the mean-field theory for a SPB concentration of $[P]_0=6.01\times10^{14}$ m^{-3}. The solid line shows the prediction of $\tilde{V}_{max}$. The broken line is calculated by increasing the prediction by 15%.

the reaction-limited coagulation regime where $W>1$ to the diffusion-limited fast coagulation regime in which $W=1$. Hence, the lanthanum concentration of 0.5 ± 0.1 mmol/l marks the critical coagulation concentration (ccc) of the SPB. The same ccc was also found for another anionic SPB, with similar bare charge Q_b, in the presence of $LaCl_3$ [2] despite the differences between the two SPB systems in regards to grafting density and contour length of the polyelectrolyte chains. Note that increasing $[P]_0$ with decreasing lanthanum concentration is necessary to maintain a good signal to noise ratio during light scattering experiments while the coagulation rate is reduced.

Figure 4 also shows the theoretical prediction of W from the variational free energy approach given in Sec. III B (solid line). It slightly deviates from the experimental measurements, but considering the experimental error it still predicts the transition point of the ccc up to an accuracy of 0.2 mmol/l of added salt. Note that this comparison is done without any adjustable parameters. A better overall matching of the theoretical prediction can be achieved assuming a 15% increase of the predicted net charge (Fig. 4, broken line). Thus, the mean-field model underestimates the charge density and the number of counterions evading the brush layer, especially in the case of low salt concentrations.

The experimental fast coagulation rate constant $k_{11,fast}$ of the SPB in lanthanum solution is $(4.1\pm0.1)\times10^{-18}$ m^3/s. This value is in very good agreement with the value found previously [2], but smaller than the theoretical von Smoluchowski value of 12.2×10^{-18} m^3/s. The present value also agrees well with data found in the literature for systems of comparable hydrodynamic dimensions [23,24,65,66]. In agreement with our earlier study [2], and with the work of Mei and co-workers [16,19], we find that the initial hydrodynamic radius $R_h(0)$ stays constant for all lanthanum concentrations. This $R_h(0)$ corresponds to the radius of the SPB after the addition of salt, but before coagulation. Thus, even at the lowest salt concentration of 0.16 mmol/l a full collapse of the polyelectrolyte shell of the SPB occurs immediately.

Taking into account a hydrodynamic core radius of (125 ± 2) nm and using (137 ± 3) nm for $R_{h,csl}$, the hydrodynamic thickness L of the collapsed shell layer results to (12 ± 4) nm. In our previous study we found $L=7$ nm for a similar SPB in the presence of $LaCl_3$ [2]. Considering the differences in the brush parameters of the two SPB systems and the experimental error of $R_{h,csl}$, the agreement is satisfactory. However, the brush thickness obtained from the variational free energy calculations is much smaller than the experimental value ($L=3.8$ nm at $c_0\approx0.2$ mmol/l). We attribute this discrepancy mainly to the various simplifications of the theoretical model employed here.

C. Force balance: Repulsive energy and effective surface charge

From the stability measurements, we can then calculate the height of the maximum value of $V(r)$ [Fig. 1(c)], which is the prefactor $\tilde{V}_{max}=V_{max}/k_BT$ in Eq. (16). Using Eq. (16) we fit $\tilde{V}_{max}$ to the values of the stability ratio determined in our light scattering experiments for all $LaCl_3$ concentrations. Plotting $\tilde{V}_{max}$ as a function of c_0 reveals a decrease of $\tilde{V}_{max}$ with increasing counterion concentration (Fig. 5). This is due to a charge regulation effect taking place inside the polyelectrolyte shell layer, which occurs as the polyelectrolyte brush becomes more and more neutralized by lanthanum counterions (Sec. III B). Figure 5 demonstrates that the repulsive

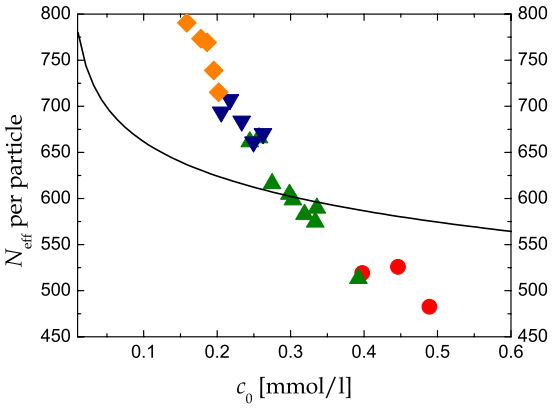

FIG. 6. (Color online) Number of effective charges per SPB particle for four different SPB concentrations $[P]_0$: 8.00×10^{15} m^{-3} (diamonds); 2.00×10^{15} m^{-3} (reversed triangles); 6.01×10^{14} m^{-3} (triangles); 3.00×10^{14} m^{-3} (circles). The data points were calculated from the experimental determined values of the prefactor V_{max} using a thickness of the collapsed brush layer of 12 nm. The solid line is the prediction from the mean-field theory for a SPB concentration of $[P]_0=6.01\times10^{14}$ m^{-3}.

energy of the system at $r=R_h$ can be accurately measured in units of k_BT for high values of $\tilde{V}_{max}$. However, for low values of $\tilde{V}_{max}$ the experimental error is higher due to two main reasons: The correction function for the hydrodynamic drag $B(h)$ and the van der Waals terms, H_c and H_s, are less exact at small particle separations, and the highest possible force resolution is on the order of k_BT. Thus, $\tilde{V}_{max}$ is affected by a larger error in this regime.

Figure 5 also shows the comparison between theory (Sec. III B) and experiment. The prediction of $\tilde{V}_{max}$ that involves no fitting parameters reveals good agreement at higher salt concentrations. However, at lower salt concentrations better agreement is achieved if the predicted value of the charge density Σ is increased by 15% (dashed line in both Figs. 4 and 5). Therefore, the theory predicts $\tilde{V}_{max}$ of the SPB within an error of no more than 4 units of k_BT at lanthanum concentrations of 0.16 to 0.5 mmol/l.

From the experimental data of $\tilde{V}_{max}$, the number of effective charges N_{eff} per SPB particle can also be calculated. According to Eq. (9), V_{max} is proportional to the square of the surface potential of the SPB particles. From the surface potential, the surface charge density of the particles is attainable using the approximate analytic expression for 3:1 salts according to Zhou [52]. We then calculated the number of effective charges per SPB as a function of c_0 using $R_{h,csl}=137$ nm for the particle size. The results are shown in Fig. 6.

Through comparing Figs. 5 and 6 we can see that at 450–500 effective charges the electrostatic repulsion between the SPB particles approaches the value of 1 k_BT. Here the coagulation becomes diffusion limited. In the slow coagulation regime, N_{eff} rises to 800 charges per particle at $c_0=0.16$ mmol/l, corresponding to 8.5 units of k_BT and a stability ratio of about 700. Thus, the present experimental approach enables us to measure the decrease of the maximum of the repulsive interparticle energy with an accuracy on the order of k_BT. The number of effective charges per SPB particle can be measured within $\pm20\%$.

This data is in the range of the theoretical prediction, as demonstrated in Fig. 6 (lines). At first sight, the comparison of the experimental and theoretical values for the effective charge and its dependency on added multivalent salt is not satisfactory. However, given the fact that the bare charge of the SPB is on the order of two million charges per SPB ($Q_b\approx1.9\times10^6$), its reduction to 500–800e at lanthanum concentrations of less than 0.5 mmol/l confirmed by experiments and theory is remarkable.

V. CONCLUSION

We presented a detailed account of an investigation related to repulsive forces between colloidal spherical polyelectrolyte brushes in aqueous solutions of trivalent ions. Using accurate measurements of the rate of coagulation, the strength of the repulsive potential could be measured down to values of the order of k_BT ("microsurface potential measurements"). The experimental data could be modeled in terms of a simple mean-field theory that accounts for the drastic reduction of the effective charge of the brushes by trivalent ions. The comparison of theory and experimental data demonstrates that the weakening of electrostatic repulsion can be understood on a quantitative level. Moreover, the MSPM has been shown as a reliable method for assessing weak repulsion between colloidal particles.

ACKNOWLEDGMENTS

R.F., P.P., and M.T. gratefully acknowledge support for this work from the National Science Foundation Grants No. DMR-0520415 and No. DMR-0710521 (Materials World Network). M.B. gratefully acknowledges support by the Deutsche Forschungsgemeinschaft. C.S. thanks the Elite Study Program Macromolecular Science in the Elite Network Bavaria and the Bavarian Graduate Support Program for financial support during this work. C.S and M.B. gratefully acknowledge the Bavarian California Technology Center BaCaTec for financial support of this joined project. The work at Berkeley was supported by the Laboratory Directed Research and Development Program of Lawrence Berkeley National Laboratory under the Department of Energy Contract No. DE-AC02-05CH11231.

[1] S. W. Swanton, Adv. Colloid Interface Sci. **54**, 129 (1995).
[2] C. Schneider, A. Jusufi, R. Farina, F. Li, P. Pincus, M. Tirrell, and M. Ballauff, Langmuir **24**, 10612 (2008).
[3] W. B. Russel, D. A. Saville, and W. R. Schowalter, *Colloidal Dispersions* (Cambridge University Press, Cambridge, England, 2001).
[4] B. V. Derjaguin and L. Landau, Acta Physicochim. URSS **14**, 633 (1941).
[5] E. J. W. Verwey and J. T. G. Overbeek, *Theory of the Stability of Lyophobic Colloids* (Elsevier, Amsterdam, 1948).
[6] D. F. Evans and H. Wennerström, *The Colloidal Domain* (Wiley-VCH, New York, 1999).
[7] T. Tadros, Adv. Colloid Interface Sci. **46**, 1 (1993).
[8] M. Ballauff, Prog. Polym. Sci. **32**, 1135 (2007).
[9] M. Ballauff, Curr. Opin. Colloid Interface Sci. **11**, 316 (2006).
[10] P. Pincus, Macromolecules **24**, 2912 (1991).
[11] O. V. Borisov, T. M. Birshtein, and E. B. Zhulina, J. Phys. II **1**, 521 (1991).
[12] X. Guo and M. Ballauff, Phys. Rev. E **64**, 051406 (2001).
[13] X. Guo and M. Ballauff, Langmuir **16**, 8719 (2000).
[14] M. Balastre, F. Li, P. Schorr, J. Yang, J. W. Mays, and M. V. Tirrell, Macromolecules **35**, 9480 (2002).
[15] I. E. Dunlop, W. H. Briscoe, S. Titmuss, R. M. J. Jacobs, V. L. Osborne, S. Edmondson, W. T. S. Huck, and J. Klein, J. Phys. Chem. B **113**, 3947 (2009).
[16] Y. Mei, K. Lauterbach, M. Hoffmann, O. V. Borisov, M. Ballauff, and A. Jusufi, Phys. Rev. Lett. **97**, 158301 (2006).
[17] A. Jusufi, C. N. Likos, and M. Ballauff, Colloid Polym. Sci. **282**, 910 (2004).
[18] R. Konradi and J. Rühe, Macromolecules **38**, 4345 (2005).
[19] Y. Mei, M. Hoffmann, M. Ballauff, and A. Jusufi, Phys. Rev. E **77**, 031805 (2008).
[20] M. Hoffmann, A. Jusufi, C. Schneider, and M. Ballauff, J. Colloid Interface Sci. **338**, 566 (2009).
[21] F. Li, P. Schorr, M. V. Tirrell, and J. Mays, Polym. Prepr. (Am. Chem. Soc. Div. Polym. Chem.) **46**, 377 (2005).
[22] L. Hanus, R. Hartzler, and N. Wagner, Langmuir **17**, 3136 (2001).
[23] H. Holthoff, S. U. Egelhaaf, M. Borkovec, P. Schurtenberger, and H. Stricher, Langmuir **12**, 5541 (1996).
[24] S. H. Behrens, D. I. Christl, R. Emmerzael, P. Schurtenberger, and M. Borkovec, Langmuir **16**, 2566 (2000).
[25] J. N. Israelachvili, J. Colloid Interface Sci. **44**, 259 (1973).
[26] E. E. Meyer, K. J. Rosenberg, and J. N. Israelachvili, Proc. Natl. Acad. Sci. U.S.A. **103**, 15739 (2006).
[27] D. G. Grier, Nature (London) **424**, 810 (2003).
[28] K. Kegler, M. Salomo, and F. Kremer, Phys. Rev. Lett. **98**, 058304 (2007).
[29] G. Dominguez-Espinosa, A. Synytska, A. Drechsler, C. Gutsche, K. Kegler, P. Uhlmann, M. Stamm, and F. Kremer, Polymer **49**, 4802 (2008).
[30] P. M. Claesson, T. Ederth, V. Bergeron, and M. W. Rutland, Adv. Colloid Interface Sci. **67**, 119 (1996).
[31] S. G. Bike, Curr. Opin. Colloid Interface Sci. **5**, 144 (2000).
[32] J. Y. Walz, Curr. Opin. Colloid Interface Sci. **6**, 600 (1997).
[33] H. J. Butt, B. Cappella, and M. Kappl, Surf. Sci. Rep. **59**, 1 (2005).
[34] J. Ralston, I. Larson, M. W. Rutland, A. A. Feiler, and M. Kleijn, J. Macromol. Sci., Pure Appl. Chem. **77**, 2149 (2005).
[35] W. A. Ducker, T. J. Senden, and R. M. Pashley, Nature (London) **353**, 239 (1991).
[36] X. Guo, A. Weiss, and M. Ballauff, Macromolecules **32**, 6043 (1999).
[37] M. Schrinner, B. Haupt, and A. Wittemann, Chem. Eng. J. **144**, 138 (2008).
[38] J. H. Kim, M. Chainey, M. S. El-Aasser, and J. W. Vanderhoff, CJ. Macromol. Sci., Pure Appl. Chem. **30**, 171 (1992).
[39] W. Brown, *Light Scattering* (Clarendon, Oxford, 1996).
[40] H.-G. Elias, *Macromolecules* (Wiley-VCH, Weinheim, 2006).
[41] F. H. Spedding and M. J. Pikal, J. Phys. Chem. **70**, 2430 (1966).
[42] H. Holthoff, M. Borkovec, and P. Schurtenberger, Phys. Rev. E **56**, 6945 (1997).
[43] R. J. Hunter, *Foundations of Colloid Science*, 2nd ed. (Oxford University Press, New York, 2004).
[44] M. von Smoluchowski, Phys. Z. **17**, 557 (1916).
[45] M. von Smoluchowski, Z. Phys. Chem. **92**, 129 (1917).
[46] E. P. Honig, G. J. Roebersen, and P. H. Wiersema, J. Colloid Interface Sci. **36**, 97 (1971).
[47] J. N. Israelachvili, *Intermolecular and Surface Forces* (Academic Press, New York, 1998).
[48] Converting the value of V_{max} at $c_0=0.16$ mM into the corresponding surface potential Ψ_0 gives $\kappa R_h=13.7\gg 1$ and $e\Psi_0/k_BT=0.29<1$.
[49] J. Gregory, J. Colloid Interface Sci. **83**, 138 (1981).
[50] R. Tadmor, J. Phys.: Condens. Matter **13**, L195 (2001).
[51] J.-P. Hsu and Y.-C. Kuo, J. Colloid Interface Sci. **167**, 35 (1994).
[52] S. Zhou, J. Colloid Interface Sci. **208**, 347 (1998).
[53] A. Jusufi, C. N. Likos, and H. Lowen, Phys. Rev. Lett. **88**, 018301 (2002).
[54] A. Jusufi, C. N. Likos, and H. Lowen, J. Chem. Phys. **116**, 11011 (2002).
[55] R. Ni, D. Cao, W. Wang, and A. Jusufi, Macromolecules **41**, 5477 (2008).
[56] A. Jusufi, J. Chem. Phys. **124**, 044908 (2006).
[57] W. Groenewegen, S. U. Egelhaaf, A. Lapp, and J. R. C. van der Maarel, Macromolecules **33**, 3283 (2000).
[58] M. Roger, P. Guenoun, A. Muller, L. Belloni, and M. Delsanti, Eur. Phys. J. E **9**, 313 (2002).
[59] N. Dingenouts, M. Patel, S. Rosenfeldt, D. Pontoni, T. Narayanan, and M. Ballauff, Macromolecules **37**, 8152 (2004).
[60] The difference between a uniform and nonuniform brush density at $r=R_c$ and the edge of the brush at $r=R_h$ is below 10%, if the density profile decays with r^{-2}, and $<5\%$ in the case of a decay with r^{-1}.
[61] S. Alexander, J. Phys. (Paris) **38**, 977 (1977).
[62] P. G. de Gennes, Macromolecules **13**, 1069 (1980).
[63] A. Zaccone, H. Wu, M. Lattuada, and M. Morbidelli, J. Phys. Chem. B **112**, 1976 (2008).
[64] H. Holthoff, A. Schmitt, A. Fernández-Barbero, M. Borkovec, M. Á. Cabrerízo-Vílchez, P. Schurtenberger, and R. Hidalgo-Álvarez, J. Colloid Interface Sci. **192**, 463 (1997).
[65] H. Sonntag and K. Strenge, *Coagulation and Structure Formation* (VEB Deutscher Verlag der Wissenschaften, Berlin, 1987).
[66] J. H. van Zanten and M. Elimelech, J. Colloid Interface Sci. **154**, 1 (1992).